Strain analysis of a seismically-imaged mass-transport complex (MTC), offshore Uruguay

Michael J. Steventon[1*], Christopher A-L. Jackson[1], David M. Hodgson[2] & Howard D. Johnson[1]

[1]Basins Research Group (BRG), Department of Earth Science & Engineering, Imperial College, Prince Consort Road, London, SW7 2BP, UK

[2]School of Earth and Environment, University of Leeds, Leeds, LS2 9JT, UK

*Corresponding author: michael.steventon13@imperial.ac.uk

ABSTRACT

Strain style, magnitude, and distribution within mass-transport complexes (MTCs) is important for understanding the process evolution of submarine mass flows and for estimating their runout distances. Structural restoration and quantification of strain in gravitationally-driven passive margins have been shown to approximately balance between updip extensional and downdip compressional domains; such an exercise has not yet been attempted for MTCs. We here interpret and structurally restore a shallowly buried (c. 1500 mbsf) and well-imaged MTC, offshore Uruguay using a high-resolution (12.5 m vertical and 15x12.5 m horizontal resolution) 3D seismic-reflection survey. This allows us to characterise and quantify vertical and lateral strain distribution within the deposit. Detailed seismic mapping and attribute analysis shows that the MTC is characterised by a complicated array of kinematic indicators, which vary spatially in style and concentration. Seismic-attribute extractions reveal several previously undocumented fabrics preserved in the MTC, including internal shearing in the form of sub-orthogonal shear zones, and fold-thrust systems within the basal shear zone beneath rafted-blocks. These features suggest multiple phases of flow and transport directions during emplacement. The MTC is characterised by a broadly tripartite strain distribution, with extensional (e.g. normal faults), translational and compressional (e.g. folds and thrusts) domains, along with a radial frontally emergent zone. We also show how strain is preferentially concentrated around intra-MTC rafted-blocks due to kinematic interaction between these features and the underlying basal shear zone. Overall, and even when volume loss within the frontally emergent zone is excluded, a strain difference between extension (1.6-1.9 km) and contraction (6.7-7.3 km) is calculated. We attribute this to a combination of distributed, sub-seismic, 'cryptic' strain, likely related to de-watering, grain-scale deformation, and related changes in bulk sediment volume. This work has implications for assessing MTCs strain distribution and provides a practical approach for evaluating structural interpretations within such deposits.

Keywords: mass-transport deposit (MTD), submarine landslide, Punta del Este, Oriential del Plata, kinematic indicators, seismic geomorphology, deep-water depositional systems

1. INTRODUCTION

Mass-transport complexes (MTCs) are gravity-driven shear failure deposits resulting from creep, slide, slump, and debris flow processes (e.g. Dott 1963; Nardin 1979; Nemec 1990; Weimer 1990; Posamentier & Martinsen 2011). Numerous studies have demonstrated the key role that MTCs play in (1) continental margin construction, (2) petroleum systems development, and (3) geohazard prediction (e.g. Posamentier & Kolla 2003; Weimer & Shipp 2004; Moscardelli et al. 2006; Armitage & Stright 2010; Meckel 2011; Clare et al. 2017). *Qualitative* descriptions of the structure and kinematic indicators within MTCs are well-documented by many seismic-reflection and outcrop-based works (e.g. Prior et al. 1984; Masson et al. 1993; Frey-Martínez et al. 2006; Gee et al. 2006; Bull et al. 2009; Sobiesiak et al. 2017; Alsop et al. 2018; Ortiz‐Karpf et al. 2018). It is important to also have a more *quantitative* understanding of how strain is distributed in MTCs if we are to understand how partially lithified sediment deform during remobilisation on submarine slopes. Yet, to-date, such a quantitative assessment of the strain distribution within MTCs has been limited by data type and quality: outcrop studies lack continuous observations from the extensional to compressional domain (e.g. Martinsen & Bakken 1990; Sharman et al. 2017), and seismic-reflection data are limited by a lack of internal bedding preservation, or the inability of these data to resolve any bedding that may be present (e.g. Frey-Martínez et al. 2006). A systematic characterisation and quantitative restoration of intra-MTC strain thus requires relatively high-resolution 3D seismic-reflection data that image the full extent of a large MTC.

In contrast, structural restoration and quantification of strain across very large (i.e. up to 500 km in dip extent; up to 6 km thick) gravitationally unstable continental margins is common. These systems typically develop on shale or salt detachments (e.g. Hudec & Jackson 2004; Butler & Paton 2010) and demonstrate that up-dip extension, typically accommodated by normal faulting, is broadly balanced downdip by folding and thrusting (Rowan et al. 2004). Gravitational margins can also show a component of vertical strain partitioning where deeper layers of stratigraphy accommodated increasing amounts of strain (e.g. Butler & Paton 2010). Similarly, in MTCs it may be suggested that upslope extension is approximately balanced by downslope contraction (e.g. Lewis 1971; Farrell 1984), and that pre-failure compaction and penetrative strain (see Burberry 2015) may play a role in how strain is concentrated vertically. However, despite MTCs containing a similar overall morphology to larger gravitational margins, previous studies have not quantified strain distribution across an entire MTC.

Here, we undertake a detailed strain analysis of a shallowly buried and thus well-imaged MTC (c. 1500 mbsf) identified in a high-resolution 3D seismic-reflection survey, offshore Uruguay (Fig. 1). The seismic-interpretation provides a framework for constructing a 2D structural model and quantifying the lateral strain. The specific objectives are as follows: (1) to assess intra-MTC strain distribution, (2) to quantify extensional and compressional strain, (3) to test the hypothesis that MTC strain is best defined by a broadly tripartite strain distribution, (4) to characterise vertical and longitudinal strain distributions within the MTC, and (5) to investigate how strain is partitioned around major structures within and beneath the MTC. Our approach will aid in detailed extraction of MTCs structural complexities and support the assessment of seal integrity beneath and within these deposits.

2. GEOLOGICAL SETTING

Sedimentary basins offshore Uruguay form part of the Gondwanan break-up cycle and subsequent northward propagation of South Atlantic opening during the Late Jurassic-Early Cretaceous (Rabinowitz & LaBrecque 1979; Nürnberg & Müller 1991) (Fig. 1). Rifting occurred in two main phases: (i) an initial Jurassic phase that failed to produce oceanic crust, and which resulted in the formation of a NW-trending rift that is recorded in the nearshore Punta del Este and Argentine basins;

and (ii) a second, Early Cretaceous phase, which is recorded in the distal Punta del Este, Pelotas and Brazilian basins, where it is related to formation of a NE-trending rift (Soto et al. 2011).

Four main sedimentary megasequences are identified offshore Uruguay: (i) a Paleozoic pre-rift sequence, (ii) a Jurassic-Early Cretaceous syn-rift sequence, (iii) a Barremian-Aptian transition sequence, and (iv) a Aptian-Holocene post-rift sequence (Morales et al. 2017). This study focuses on the up to 3 km thick, Neogene to Holocene post-rift sequence. In the Punta del Este basin, Neogene to Holocene deposition occurred in association with overall progradation of large (up to 1.5 km tall) clinoforms. The MTC studied here occurs downdip of these clinoforms, above a regional Miocene unconformity (Conti et al. 2017) (Fig. 2).

3. DATASET & METHODS

3.1. Dataset and seismic interpretation

The 3D pre-stack depth migrated (PSDM) seismic reflection survey used in this study covers an area of *c.*13,000 km^2. The data are SEG reverse polarity standard (European polarity, i.e. an increase in acoustic impedance = trough), have a stacking bin spacing of 15×12.5 m and a vertical resolution (limit of separability) of c.12.5 m at 2.5 km depth. A shallowly buried (c. 1500 mbsf), and thus seismically well-imaged, MTC was selected for detailed seismic characterisation and strain analysis (Fig. 1). We mapped the base and top of the MTC, in addition to numerous internal faults and stratigraphic reflections. Mapping enabled construction of stratigraphic thickness (isopach) maps, extraction of kinematic indicators, and calculation of intra-MTC strain. No wells penetrate the MTC, thus we cannot constrain the lithology or precise age of emplacement.

3.2. Seismic attribute analysis

Several geometric-, amplitude-, and frequency-based attributes were used to assess the external and internal morphology of the MTC. Seismic variance (coherency) was calculated based on the Van Bemmel & Pepper (2000) edge detection method, allowing better imaging and mapping of discontinuities, such as intra-MTC faults. Seismic attributes are often sensitive to noise within the input data (Chopra & Marfurt 2008). Hence, the raw reflectivity data was conditioned by a single layer-parallel smoothing iteration before variance attribute computation (see Randen & Sønneland 2005). We also used ant-tracking, a method of enhancing discontinuities in 3D seismic data, to image and map fracture networks (Randen 1998; Randen et al. 2001). We also applied spectral decomposition to the raw reflectivity data; this splits the seismic signal into narrow frequency bins (i.e. low, mid and high) that, when blended together, highlight structural and stratigraphic heterogeneities (see Partyka et al. 1999). Several grid-based attributes, such as dip magnitude and root-mean squared (RMS) amplitude, were also employed to aid interpretations. In addition to grid-based surface attribute extractions, we also undertook iso-proportional slicing within the MTC to capture internal structural fabrics (see Zeng et al. 1998).

3.3. Decompaction and strain analysis

A kinematic strain analysis of the MTC was undertaken to assess longitudinal (i.e. sediment transport-parallel) strain. Strain analysis was used to test the validity of the seismic interpretation (i.e. does the section balance and preserve rock volume, thickness, length, etc.) and to quantify strain distribution within the MTC (Dahlstrom 1969; Hossack 1979; Lingrey & Vidal-Royo 2015). The MTC studied here is defined by packages of chaotic reflections (e.g. Posamentier & Kolla 2003), thus it was not possible

to interpret internal reflections across the entire deposit and we therefore undertake a 2D rather than 3D restoration. We assume only plane-strain deformation (i.e. extension and shortening parallel to the bulk sediment transportation direction) and preservation of line-length. However, out-of-plane strain, in addition to volume loss due to vertical transport (re-suspension) of material out-of-section could occur. To help mitigate these effects, we orientated the sections parallel to the dominant MTC transport direction through identification of kinematic indicators such as lateral margins (Fig. 3A). Due to the component of ductile strain within MTCs, simple shear and flexural slip methods have also been tested and compared with the line-length approach to quantify model sensitivities (Lingrey & Vidal-Royo 2015).

Before calculating longitudinal strain, the MTC was decompacted to remove the effects of volume decrease driven by burial-related porosity reduction. Constraining pre-compaction thickness, and thus immediately post-emplacement structural geometries of intra-MTC faults and folds, allows for a more accurate calculation of corrected strain magnitudes. Backstripping of the overburden was undertaken on a layer-by-layer basis (three layers in total). As input to the decompaction process we assumed initial surface porosities of 0.63 and 0.49, and rates of porosity decay of 0.51 and 0.27 Km^{-1} for shale and sandstone respectively. This is based on the Sclater & Christie (1980) decompaction curve ($\phi = \phi_0(e^{-cz})$), where ϕ/ϕ_0 relates to present-day and surface porosities, respectively. The MTC-dominated overburden is assumed to have the same lithological characteristics as the studied, more deeply buried MTC (Fig. 4-A). The composition of the MTC (45% clay, 45% silt, 10% sand) was estimated from a shallow core sample (GeoB13860-1) taken from a seabed MTC on the Uruguayan margin (Krastel et al. 2011). Our estimated composition is thus comparable to MTCs observed at outcrop (e.g. Pickering & Corregidor 2005), although MTCs are, by their nature, compositionally highly variable and can in some cases be sand/sandstone-rich (e.g. Meckel 2011; Sharman et al. 2017).

The strain (e) of folded and faulted pre-kinematic strata can be approximated by summing the individual segments of a horizon ($L_0 = H_1 + H_n$) and comparing this to the present length (L_1) (1):

$$e = (L_1 - L_0)/L_0) \quad (1)$$

The calculated strain is at best a minimum estimate, as only macro-scale structures are identifiable and thus restorable (i.e. sub-seismic faulting and folding cannot be explicitly accounted for using this method; e.g. Marrett & Allmendinger (1992)). Thus, a strain mismatch of 2-60% may be ascribed to variables that cannot be identified using seismic data; we discuss later potential ways in which we can mitigate these uncertainties (Marrett & Allmendinger 1992; Burberry 2015). Structural restoration and strain analysis also carry interpretation errors, with our interpretation of structures being subjective and non-unique, and likely biased towards our previous geological experiences and concepts (see Bond et al. 2007). Variations in interpretation of fault-horizon cut-offs may also produce bed length errors of up to ±10% (Judge & Allmendinger 2011). Furthermore, based on arguments outlined below, we assume downdip shortening is accommodated by discrete thrusts that are flanked by footwall synclines and hangingwall anticlines. In this case, the magnitude of shortening across an individual thrust is taken as the reverse heave (i.e. horizontal component of deformation) across a stratigraphic horizon/seismic reflection. However, as noted in field examples, downdip shortening could be accommodated by the formation of isoclinal folds rather than discrete thrusts (e.g. Sharman et al. 2015) (see Supplementary 4). In this case, there is no discrete thrust fault, and reverse heave cannot be calculated; thus, the magnitude of shortening equals the difference between the original and folded line lengths.

4. SEISMIC CHARACTERISATION OF THE MTC

4.1. General characteristics and nature of bounding surfaces

The studied MTC is dominated by low-amplitude, chaotic seismic reflections, with a high-amplitude, semi-continuous basal reflection that caps a sequence of older-MTCs and polygonally-faulted mudstones (Fig. 4). The high-amplitude basal reflection is interpreted as a basal shear surface, representing a *kinematic boundary layer* (*sensu* Butler et al. 2016) or zone, upon which the MTC was translated and ultimately deposited (Varnes 1978; Martinsen 1994). The basal shear surface connects updip to a headwall scarp and downdip to a frontal ramp, which define the limit of the extensional and compressional domains, respectively. Across the majority of the MTC, the basal shear surface is laterally continuous and concordant with underlying stratigraphy, except for where it cuts up through stratigraphy at the lateral margins. Locally, however, there is considerable relief (up to 460 m) along the basal shear surface in the form of steps and ramps, displaying variations in reflection frequency and polarity across this relief (*sensu* Bull et al. 2009).

The top of the MTC is hummocky (vertical relief 13-65 m, angle $0\text{-}10^0$) and of highly variable reflectivity (Fig. 4). In areas undisrupted by later deposition, the top surface is expressed as a positive reflection, defining a downward decrease in acoustic impedance. Elsewhere, the reflection is either highly variable or absent with no discrete structural features (i.e. faulting or folding). We interpret the geometric irregularity and acoustic variability in the top surface to reflect a combination of (1) scouring and incision of the MTC by later mass flows, (2) a component of high yield strength of the overlying debrite, and (3) the effect of large coherent blocks (Fig. 4 & Fig. 6-A) (Hodgson et al. 2017).

Directly beneath the top surface is a highly chaotic, weakly reflective zone that lacks distinct structures such as faults or folds (Fig. 4-A, Inset 1 & 2). The highly chaotic seismic facies infills topographic lows developed between thrust-cored fold structures and shear zones present in the downdip part of the MTC (see below).This upper chaotic package abruptly thins basinward within the frontally emergent zone, downdip of the thrust-cored folds and the MTC frontal ramp. Given its chaotic seismic character, this package may represent a mud-rich debris flow deposit (i.e. a debrite), which formed *during* or *after* the MTC emplacement, an important distinction we explore in the Discussion.

The MTC is thickest (up to 550 m) and has greatest relief on its top surface along the eastern and western margins, where folding and thrusting is concentrated (Fig. 3). The MTC thins to the east-southeast due to incision and erosion by later MTCs, which limits identification of its eastern margin (Fig. 3-B & Fig. 5-A). The lateral margins of the MTC record layer-normal shear orientated approximately parallel to the palaeo-slope (Alsop & Holdsworth 2007; Debacker et al. 2009). The lateral margins are most prominent within the downdip compressional domain and are linked to both the headwall scarp and frontal ramp. They are up to 300 m high separating the MTC from surrounding undisrupted deposits and indicate a translation direction towards the south-east (118-153°).

We recognise four internal domains within the studied MTC: (i) an extensional domain, defined updip by a headwall scarp and locally containing well-imaged normal faults, (ii) a seismically chaotic translational domain, (iii) a compressional domain defined downdip by a frontal ramp and containing well-developed thrust-cored folds, and (iv) a frontally emergent domain (Fig. 4-A) (cf. Posamentier & Kolla 2003; Moscardelli et al. 2006; Lamarche et al. 2008; Bull et al. 2009; Gamboa & Alves 2016). We describe the detailed structural characteristics of these domains below.

4.2. Extensional domain

The headwall scarp bounds the updip extent of the extensional domain, being instantly recognisable in variance extraction maps as the boundary between the undeformed slope and the strongly deformed (i.e. seismically chaotic) MTC (Fig. 5-A). The headwall scarp trends NE, approximately parallel to the

palaeo-slope and rather than having the characteristic arcuate shape (cf Bull et al. 2009), is instead segmented. Numerous NE-SW-striking (i.e. broadly scarp-parallel), gently (20-35°) SE-dipping normal faults occur immediately downdip of the headwall scarp. Further downdip, towards the translational domain, these faults become progressively smaller, and thus below seismic resolution, or are truly absent. An alternative interpretation is that faults developed in this domain were overprinted during further downslope movements, disaggregating along with the matrix (Fig. 4-B). The extensional domain forms a relatively small section of the MTC, with a downdip extent of only 6.5-20 km.

4.3. Translational domain

The length and seismic character of the translational domain is highly variable along strike (Fig. 3-B and 4-C), being narrowest (<5 km) where the extensional and compressional domains almost merge, and widest (c.18 km) near the central part of the MTC, where large blocks of continuous, often high-amplitude reflections occur. Many of these blocks are deformed by normal faults, which may also deform the underlying basal shear surface (Fig. 6-A). The NNE-SSW strike of the moderately dipping (c. 35-50°) normal faults, suggests a SE-orientated minimum compressive stress (σ_3) approximately parallel to the overall MTC transport direction. Small, arcuate fold-thrust systems occur below several of these blocks within the basal shear zone (Fig. 6-A). At the base, variance and spectral decomposition extractions image the overall arcuate fold-thrust footprint, while the ant-tracking extractions reveal additional discontinuities relating to individual faults/fractures. The main mass of the block is clearly discernible as a coherent unit surrounded by a more chaotic matrix in the extractions at 150 m. At 300 m, the blocks lack coherent reflections and change to fully opaque matrix facies (Fig. 6-A). These observations suggest the blocks were transported, rather than representing remnant blocks (Jackson 2011; Gamboa & Alves 2015; Hodgson et al. 2017). The occurrence of compressional and extensional structures in the same area may reflect polyphase deformation and a strain sequence recording acceleration (i.e. normal faulting), along with translation in the basal shear zone fold-thrust system.

4.4. Compressional and frontally emergent domains

The compressional and frontally emergent domains characterise the downdip termination of the MTC (Frey-Martínez et al. 2006). In this example, the MTC climbs up the frontal ramp and becomes emergent, passing downdip into an overlying package of chaotic seismic reflections interpreted as a debrite.

The compressional domain is highly deformed and contains a well-imaged fold-thrust system and related shear zones (Figs. 4-D, 5-B, 5-D). In map view, the domain is radial, with the fold-thrust system trending 015°-195° in the east to 100°-280° in the west. The thrusts typically dip 30-40° (some up to >60°) towards the NW (i.e. updip). Displacements range from 12.5 (minimum vertical resolution) to 175 m and vary along strike, with relays (fault-linkage) forming between individual thrust segments (Fig. 6-B). The thrusts detach downwards onto the basal shear zone and can affect the entire vertical extent of the MTC, particularly towards the frontal ramp. The thrusts are flanked by and dissect hangingwall anticlines and footwall synclines. These folds are gentle-to-open, non-cylindrical, and verge downdip towards the frontal ramp (Fig. 6-B). Folds are more open above the thrust tips, and tighter where they have been dissected by their related thrust; we infer this geometry records an initial phase of fault-propagation folding and open fold formation that was superseded by a later phase of thrust propagation and fold dissection.

Two sets of shear zones are recognised, trending longitudinally (c.130°-310°) and sub-orthogonally (c. 050°-230°) to the slope (Fig. 5-B & Fig 5-D). The longitudinal shears are imaged on the top surface as narrow zones (100-150 m) infilled by chaotic seismic facies, interpreted as being derived from the overriding debrite. We infer these shear zones record the junction between segments of the MTC where

differential basinward transport velocities have produced strike-slip motions (Masson et al. 1993; Gee et al. 2005). The sub-orthogonal shears produced 'V'-shaped depressions within the MTC, with the associated zones dipping upslope to the NW (Fig. 6-B). These depressions are up to 600 m wide and spaced at 2-6 km intervals along the western margin of the MTC (Fig. 5-B). At the base of the sub-orthogonal shears, bedded segments are juxtaposed, with the depressions inferred to be filled by the overlying debrite. These shears probably reflect differing flow velocities within the basinward translating MTC (Bull et al. 2009). More specifically, individual segments appear to have interacted with the lateral margin and frontal ramp at different times during MTC emplacement. This may have caused segments (I) to (III) (see inset map Fig. 5-B) to decelerate intermittently, producing a component of right-lateral (dextral) internal shearing. Therefore, in addition to layer-normal shear, we also interpret a component of oblique compression against the western lateral margin to account for the changing orientation of the fold-thrust system (Strachan & Alsop 2006; Sharman et al. 2015).

Beyond the frontal ramp and in the distal reaches of the lateral ramps, the seismic character of the MTC changes abruptly, from well-defined, albeit folded and thrusted reflections, into dominantly chaotic reflections. We relate this change to: (1) a modification in transport dynamics from a confined to an unconfined system, allowing the MTC to spread-out laterally over the palaeo-seabed, and becoming disaggregated as it emerged (Frey-Martínez et al. 2006; Armandita et al. 2015), and (2) the incorporation of the seismically chaotic, younger debrite. As well as unconfined flow over the frontal ramp, spill-over of the MTC occurred where fold-thrusts curve towards the lateral margin in an upslope direction (Fig. 6-C).

4.5. Classification and transport direction

Based on its geometry and scale (c. 500-150 m thick, 50 km long, 2400 km^2), the MTC is classified as a *frontally emergent* (Frey-Martínez et al. 2006), *attached* MTC (*sensu* Moscardelli & Wood 2015). Furthermore, the Moore & Sawyer (2016) flow factor measure, which is a proxy for relative mobility, suggests the MTC has a low-medium mobility based on the hummocky top surface, well developed fold-thrust belt, and longitudinal shear zones. This would suggest an approximate transportation and deformational process spanning slump-slide rather than full plastic flow (Posamentier & Martinsen 2011).

We have shown that the MTC displays predictable albeit variable strain distributions, defined by a relatively narrow, updip extensional domain, a transitional domain of variable width, a relatively wide, downdip compressional domain and a frontally emergent domain. We have used the associated kinematic indicators (i.e. updip normal faults, MTC lateral margins, and intra-MTC shear zones) in combination with the regional basin setting to estimate the overall transport direction 118°-162°; i.e. broadly SE. This analysis informs where we select our dip-sections for strain analysis, which we describe in the following section (Fig. 3-A & Fig. 4).

5. STRAIN ANALYSIS

Strain analysis was undertaken on two dip-oriented sections positioned orthogonal to the transport direction and dominant fault strikes; as discussed above, our assumption of broadly plane strain should thus be valid (Fig. 4). The sections are positioned near the western margin (Section 1) and centre (Section 2) of the MTC and were chosen due to the high-quality seismic imaging within the compressional domain and the relative completeness of preservation (i.e. no later erosion by MTCs or submarine channels) (Fig. 3). In principle, updip and downdip strain within the MTC should

approximately balance (i.e. extension = contraction) if the system is kinematically self-contained (e.g. Farrell 1984; Martinsen & Bakken 1990; Alsop & Marco 2014).

5.1. Geometric model and decompaction

The geometric model underpinning the strain analysis is based directly on the seismic-scale geometry of the studied MTC, consisting of a 12-20 km wide extensional domain, a wide 20-30 km compressional domain, and a 1-2 km wide translational area lacking seismic-scale structures (Fig. 7). The input model consists of the basal shear surface, top surface, several intra-MTC surfaces, updip normal faults, and downdip thrusts. As there are no translational structures in Section 1 that could be measured, a boundary (denoted E/C in Fig. 7) was used in the model to mark the estimated mid-point between the compressional and extensional domains. In Section 2 we focus solely on the compressional domain due to the poor-imaging and lack of clear structures within the extensional domain. Hence, for Section 2 we simply aimed to understand the depth dependency of strain in the compressional domain, rather than evaluating longitudinal balancing through the entire MTC. Two definitions of the compressional domain were considered: (1) H_C, which includes the frontally emergent, debrite-dominated zone; and (2) $H_{C\text{-}f}$, which excludes this zone (Fig. 7). This distinction enabled quantification of the effect frontal emergence of material beyond distal ramps has on section balancing (e.g. Hudec & Jackson 2004).

The decompacted sections show a similar overall morphology to that presently observed, with minor geometric variations in Section 1 amplifying the extensional domain features to the north-west where overburden is thickest. After decompaction, the MTC increased in cross-sectional area by 27% (14.5 km^2 to 18.2 km^2) and 23% (19.4 km^2 to 24.5 km^2) for Sections 1 and 2, respectively.

5.2 Results

The present length of the extensional domain in Section 1 is 13.9 km, whereas the restored length, depending on the method used (i.e. simple shear, flexural slip, line-length), is 12.0-12.3 km, equating to 1.6-1.9 km (13-16% strain) of extension ($H3_E$, Table 1). For Section 1, a single intra-MTC reflection ($H3_C$) was interpreted through the compressional domain; the present-day length of this reflection is 32.3 km, whereas the restored length is 39.1-39.8 km, equating to 6.8-7.5 km (17-19% strain) of horizontal shortening (Table 1). When the frontally emergent zone ($H3_{C\text{-}f}$) is excluded, the proportion of horizontal shortening representing the compressional domain alone decreases to 6.7-7.3 km (25-26% strain). At the scale of resolution afforded by seismic refection data, Section 1 does not balance, with a deficit of 5.1-5.9 km between contraction and extension (i.e. extensional strain < shortening strain). The discrepancy increases when the frontally emergent zone is included.

For Section 2, two internal horizons were interpreted: a lower horizon, $H3c_i$, and an upper horizon, $H3c_{ii}$. The present length of $H3_{Ci}$ is 24.0 km, restoring to 31.8-32.8 km and thus yielding a horizontal shortening of 7.7-8.8 km (24-27% strain). For $H3c_{ii,}$ when the frontally emergent zone is included in the calculation the horizontal shortening is 4.8-5.3 km (14-15% strain), this changes slightly to 4.6-5.1 km (16-18% strain) when this zone is excluded ($H3c_{ii\text{-}f}$).Vertical variations in the magnitude of horizontal shortening are inferred in the MTC in Section 2, with a lower horizon ($H3_{Ci}$) having been shortened significantly more 7.7-8.8 km (24-27% strain) than an overlying, upper horizon ($H3_{Cii\text{-}f}$); we explore the possible origins of this vertical variation in strain below.

Overall, the strain analysis of Section 1 at least partly validates our seismic observations of strain distribution within the MTC (i.e. a strain distribution encompassing updip extension and downdip compression). Nevertheless, downdip shortening is more than updip extension. This suggests strain may have been accommodated by other, maybe sub-seismic processes that we cannot account for using the conventional strain analysis methods employed here. Below we discuss the potential impact of these processes.

6. DISCUSSION

This section considers the MTC structure and emplacement mechanism, and discusses the advantages, limitations, and implications of the strain analysis approach for understanding intra-MTC strain.

6.1. Mode of MTC emplacement

The occurrence of radial spreading-related thrust-cored folds, the distribution of extensional-translational-compressional domains, the presence of transported, yet still stratified blocks, and the relatively low degree of disaggregation throughout much of the MTC, suggests the deposit formed through slump-slide processes (e.g. Dott 1963; Nardin 1979; Merle 1989; Posamentier & Martinsen 2011; Moore & Sawyer 2016). The relationship between the MTC and its capping debrite may suggest one of two plausible models: Model 1 - the debrite and MTC are coeval, with the debris flow potentially initiating *in-situ* failure of underlying sediments (i.e. the MTC) (i.e. a 'shear-coupling' mechanism; Van der Merwe et al. 2009; Van Der Merwe et al. 2011), or Model 2 - the debrite is younger and thus genetically unrelated to, and simply fills relief created by the MTC (i.e. a 'loading/self-loading' mechanism). Observations that lend support to either model include: (1) the close correlation between the debrite thickness and MTC depressions (e.g. fold troughs and shear zones) and (2) the rapid thinning of the debrite beyond the frontally emergent zone.

Model 1 states the MTC was initiated by an overriding debris flow, which produces increased loading and localisation of shear stress on a mechanically weak zone (Fig. 8). This is consistent with similar observations from the field (e.g. Van der Merwe et al. 2009; Van Der Merwe et al. 2011) and from other seismic-based examples (e.g. Schnellmann et al. 2005). A similar model is proposed to trigger soft-sediment deformation within seismites, where folding is initiated by layer-parallel shear instability between stable stratified layers (i.e. Kelvin-Helmholtz instability mechanism) (Heifetz et al. 2005; Wetzler et al. 2010). The following observations support Model 1: (1) thrust-related hangingwall anticlines in the distal domain are not eroded at the base of the capping debrite and (2) no continuous erosional features such as grooves or striations are observed at the base of the MTC suggesting a limited run-out distance (Figs 4-6). We note, however, that these shear-coupling modes of emplacement have only been observed in relatively small deposits (i.e. 10-100 km^3) and not in association with much larger MTCs (i.e. 2400 km^3), prompting the question whether debris flows are able to impose sufficient shear on the seabed to trigger failure of such a large volume of material. Furthermore, if we infer the pre-failure geometry of the seabed (red dotted line in Fig. 8) and then compare the pre- (~10.5 km^2) vs post-failure (14.5 km^2) areas apparent in Section 1 (Fig. 4A), we find they do not match (i.e. post-failure volume is 38% larger), with there being more material in the downdip domain of accumulation than the updip domain of depletion. This mismatch may be explained by bulking of the MTC during emplacement, or out-of-section transport.

Model 2 states initial loading (i.e. self-loading of water saturated sediment near the seafloor) would drive the build-up of excess pore pressure, reduction of shear strength, and the initiation of slope failure, which would progressively develop downslope (Fig 8) (see Watt et al. 2012). After this initial failure, the remnant topography may then have been infilled by material deposited from later debris flows, which served to heal the depleted zone (Fig. 8). The following observations support Model 2: (1) limited frontal emergence; and (2) the formation of regularly spaced thrust fault planes, suggesting progressive imbrication (e.g. Morita et al. 2011) and the formation of thrusts that young updip (i.e. anti-dislocation, Farrell 1984). A potential caveat to Model 2 is the full preservation of hangingwall anticlines next to the thrusts; one may expect such structures to be eroded by later debris flow(s). Although this missing observed erosion may be explained by either (1) a sequence of smaller overriding debris flow(s) which

progressively healed the remnant topography without producing significant erosional truncations or (ii) minor erosion of hangingwall anticlines below seismic resolution.

From seismic observations alone, we can only present potential emplacement models. Yet, given the MTC significant length, thickness and aerial extent, a combination/hybrid mode of emplacement mechanisms including, loading, self-loading, shear coupling and shear rupture propagation (see Watt et al. 2012), may provide an more likely alternative to specific end-member models.

6.2. Intra-MTC strain

We have demonstrated that seismic-scale structures in MTCs can be extracted using modern seismic attribute techniques. This approach has allowed us to document two previously unrecognised types of intra-MTC structures: (1) internal shearing in the form of sub-orthogonal shear zones, and (2) fold-thrust systems within the basal shear zone beneath rafted-blocks.

Longitudinal (i.e. slope-parallel) shear zones have been attributed to variations in MTC transport velocities (Masson et al. 1993; Gee et al. 2005; Bull et al. 2009). The presence of such structures suggests emplacement of the MTC studied here was more complex than captured in relatively simple, single-celled models (see Farrell 1984). Instead, the shear zones suggest multiple cells were in operation during MTC emplacement. In addition to the longitudinal shear zones, there is a secondary sub-orthogonal set (i.e. slope-oblique), which support internal shearing linked to transport velocity variations oblique to the bulk sediment transport direction. This second set of shear zones seems to be intimately linked to the orientation of the western lateral margin (Fig. 5-B). Typically, lateral margins impose transtensional strain in areas of depletion (i.e. extensional domains) and transpressional strain in areas of volume increase (i.e. compressional domains) (Varnes 1978). Fleming & Johnson (1989) identify similarly orientated ‘cracks’ along the lateral margins of subaerial landslides in Utah, USA. However, to our knowledge, no such seismic-scale shear of this type has been documented in a submarine example. One interpretation may be that the sub-orthogonal shear zones record transpression within the compressional domain and could be classified as a form of Riedal shear or extensional fracture. This provides evidence for a strike-/oblique-slip component of deformation within the compressional domain of the MTC, providing further evidence that conceptual models illustrating a relatively simple tri-partite strain distribution within MTCs are oversimplified (e.g. Gamboa & Alves 2016).

Another new observation is the development of minor fold-thrust systems beneath rafted blocks (Fig. 6-A). Alves (2015) shows how large, rafted blocks may interact with basal shear zones, typically forming seismic-scale grooves (furrows) and scours. Field observations at the base of rafted blocks often show small-scale foliation and soft-sediment shear structures, and at a larger-scale, folding and injectites (Alves 2015; Hodgson et al. 2017). We document up to 100 m tall structures within the basal shear zone, with these extending across the aerial-footprint of a rafted-block recording the transportation pathway. Our observations support the notion that the base of MTCs and submarine landslides may be defined by a basal shear *zone* of distributed strain, rather than a discrete surface. The block: shear zone thickness ratio of 0.22 shown in Fig. 6A is consistent with the prediction of Alves & Lourenço (2010). Our results suggest that previously observed rafted blocks in other 3D seismic-reflection case studies may also have modified the basal shear zone to create similar discrete structures (e.g. Hodgson et al. 2017). However, limitations to the spatial resolution of seismic-reflection data may, in the past, have prevented clear imaging of these structures. Furthermore, in the field there is a risk that the fold-thrust systems underneath rafted-blocks could be misinterpreted as compressional domains within smaller unrelated MTCs. We therefore suggest that distributed strain in MTCs is substantial enough to create up to 100 m thick zones of intensely and predominantly contractionally strained strata. Furthermore,

our analysis shows that local variations in strain, which reflect block-substrate interactions, can be superimposed on longer-wavelength, MTC-scale variations in strain.

Identification of these intra-MTC structures demonstrates the way in which strain can be concentrated in discrete areas. This also illustrates why strain analysis results cannot be used in isolation to capture entire MTC strain characteristics.

6.3. Structural analysis and missing strain components

Updip extension and downdip contraction does not balance within the studied MTC. We find the compressional domain accommodates approximately 6.7-7.5 km of contraction, while the extensional domain accommodates 1.6-1.9 km of extension. Below we discuss factors that may lead to an underestimation of intra-MTC strain, including: (1) strain analysis and restoration techniques, (2) conceptual uncertainty (3) volume loss due to lateral compaction, (4) distributed strain, related to porosity reduction and dewatering, (5) focused strain on sub-seismic faults and folds, and (6) strain overprinting.

Strain analysis and restoration techniques

Variations in results between the line-length and flexural slip strain analysis methods are insignificant in the compressional domain, simply because both procedures preserve line length (Lingrey & Vidal-Royo 2015; Fossen 2016). The application of simple shear produces a greater discrepancy, with less shortening recorded in the compressional domain of Section 1, likely reflecting the method's inability to preserve line length and poor handling of steeper-dips (i.e. the fold-limbs immediately adjacent to the hangingwall and footwall cutoffs).

The results also show that definition of the dip-oriented extent of the MTCs has an impact on the compressional domains accommodated strain. Inclusion of the debrite-dominated material basinward of the frontal ramp is thus a key factor for characterising the contraction domain of an MTC strain balancing. This suggests that a "foreland" type strain zone is apparent beyond the seismically defined boundary of the MTC. This is comparable to that demonstrated at significantly larger scales on salt-rich passive margins. In these cases, extrusion of the salt-nappes has been shown to accommodate a significant proportion of shortening (see Hudec & Jackson 2004). Therefore, characterisation of the terminal emergent wedge of a frontally emergent MTC is critical for quantifying shortening.

There are several limitations inherent to strain analysis and the line-length, flexural slip and simple shear methods. Line-lengths, and hence cross-sectional areas, are unlikely to be preserved in MTCs due to penetrative strain. For example, in order to understand deformation in the distal contractional domain, in particular the impact of so-called 'cryptic' lateral compaction may require the application of area sensitive methods, such as area-depth-strain (ADS) (e.g. Schlische et al. 2014). Additionally, physical and numerical models may allow more rigorous definition of boundary conditions (e.g. porosity distributions) during remobilisation of semi-lithified sediments (e.g. Wang et al. 2017).

Conceptual uncertainty

Interpretation, as shown by Bond et al. (2007), is prone to conceptual uncertainty, based on an interpreters prior geological knowledge. This concept is particularly important to consider when using remote sensing data such as seismic-reflection surveys, as often no direct sampling (i.e. well penetration) is available. Although we are confident that the compressional domain of the MTCs is composed of a thrust-cored fold system, we recognise that an alternative interpretation of shortening by

near-isoclinal folding model, is also plausible (see Sharman et al. 2015). Invoking the latter model for Section 1 shows that the apparent shortening increases significantly, from 18 to 43% and 26 to 54%, for $H3_c$ and $H3_{c\text{-}f}$ respectively (Table 2). This increase can be explained by the additional line-length of middle fold limbs in a near-isoclinal folding model. This demonstrates the significance of the geological model applied to strain analysis calculations, and may suggest that another way in which we may be underestimating shortening in the downdip domain.

Sub-seismic strain

Despite the relatively high vertical and lateral resolution of our seismic-reflection dataset (12.5 by 12.5-15 m), not all intra-MTC structures can be imaged, most notably (1) distributed, cryptic features associated with penetrative strain (e.g. intergranular deformation), (2) discrete fractures and folds, and (3) the definition of hangingwall-footwall cutoffs verses near isoclinal folds. Hence, the estimations of extension and compression represent minima values, since the strain analysis methods capture only seismic-scale deformation (cf. Kautz & Sclater 1988; Marrett & Allmendinger 1992; Walsh et al. 1996; Burberry 2015; Dalton et al. 2017).

Penetrative strain typically accommodates between 2-30% of overall shortening in horizontal shortening-related analogue models (Koyi et al. 2004; Burberry 2015). The amount of penetrative strain decreases away from thrust belts (Craddock & van der Pluijm 1989), with the magnitude of layer-parallel shortening increasing with depth (Koyi 1995). In physical models, the increase in shortening with depth (c.19%) is accommodated by (1) a decrease in bed-length, (2) an area-loss through lateral compaction in deeper layers, (3) layer-normal thickening of shallower layers, and (4) increased displacement on thrusts (Koyi 1995; Koyi et al. 2004; Groshong et al. 2012). We make similar observations in the up to 550 m thick MTC studied here, with strain increasing with depth from $H3_{ii\text{-}f}$ (18%) to $H3_i$ (27%), at least in Section 2. This suggests similar depth dependant layer-parallel shortening, perhaps related to one or a combination of the processes listed above. Physical models only record grain-grain displacement and, therefore, penetrative strain estimates are only considered a minima of that occurring in natural systems (Burberry 2015). The mechanisms of penetrative strain within the MTC are likely to include the following: (1) grain-grain displacements, (2) dewatering, minor folding and faulting, and (3) other minor structures only observable in the field (e.g. Sobiesiak et al. 2017). Similar studies of high-porosity (40-70%) sediments at equivalent depths (i.e. 700 mbsf) experience horizontal ductile shortening of c. 12% before the formation of discrete structures (Henry et al. 2003). It is not possible to quantify the degree of lateral porosity and fluid loss within the MTC without calibration from well data. However, we can assume that some component of shortening related to these mechanisms is being overlooked on a seismic-scale study. Therefore, we may expect penetrative strain in the compressional domain of the studied MTC to be larger than that estimated by physical models.

It is well known that seismic-reflection based restoration and strain analysis studies may underestimate true strain; for example, these data may underestimate 15-60% of the true extensional strain occurring in rift basins (Marrett & Allmendinger 1992; Walsh et al. 1996). This error is generally ascribed to seismic-resolution limitations, most notably (1) "small" fault populations, which contribute significant amounts to extension, and (2) ductile strain components of extensional faults, which are commonly overlooked. Similar missing extensional components are expected in this MTC. Assuming normal fault populations follow fractal size distributions, it is possible to estimate the missing extensional strain using the heave and number of observable faults (Marrett & Allmendinger 1992; Knott et al. 1996). Using this relationship, we can estimate extension of sub-seismic extensional faults (h_{sf}) by measuring heaves on the observable faults (h_{lf}), where N = number of faults and C = characterises the relative numbers of sub-seismic to observable faults (Marrett & Allmendinger 1992).

$$h_{sf} = h_{lf} \frac{C}{1-C}(N+1)\left(\frac{N}{N+1}\right)^{1/N} \quad (2)$$

The above equation is very sensitive to the linear relationship between N and displacement, and hence variations in exponent C. When using 3D-seismic reflection data, Gauthier & Lake (1993) found that, in most cases, C = ~1, ranging from 0.8-1.5. For Section 1, we estimate between 17-40% additional extension from sub-seismic faulting, assuming C = 0.9-1.1, h_{lf} = 1.88 km and N = 13. This value is in line with other estimates of missing extensional strain and eloquently demonstrates the limitations of palinspastic restoration and strain analysis.

With the recognition of missing strain components, we are inevitability underestimating shortening and extension. However, even if we include these estimated values for these missing strain components (compression +30%, extension +17-40%), we could not balance the section analysed here. Fieldwork, and physical and numerical modelling may be required to validate sub-seismic balancing of MTCs.

Overprinting, polyphase deformation and cell flow models

Classic single-cell dislocation models describe the idealised case of a single MTC sheet, referred to as a "cell", propagating downslope, with up-dip extension balanced by down-dip contraction (Lewis 1971; Farrell 1984). The model suggests an initial point of failure along a weak detachment layer, with compression occurring downslope and extension upslope of this point (Farrell 1984). This concept is useful for gaining a first-order understanding of MTCs gross-structure but, as field studies have shown, in some cases is oversimplified (e.g. Alsop & Marco 2014).

Our MTC displays many of the features proposed by single-celled models such as (1) downslope thrust patterns, and (2) basinward fold-vergence. However, as Farrell (1984) notes in the original model, a component of "anti-dislocation" (i.e. propagation of strain through the MTC as it ceases translation) may cause overprinting of primary structures. The overprinting would come about due to the termination of shear failure on the basal shear surface occurring at either the head or toe of the MTC. In practical terms, this would mean (1) if the toe stopped translating basinward, or was at least moving basinward at a lower velocity than the updip domain, then contractional strain would propagate upslope, or (2) if the head stopped translating basinward, or was at least moving basinward at a lower velocity than the downdip domain, then extensional strain would propagate downslope, until the full mass of the MTC has come to rest. This leads to the formation of additional structures such as shear fractures, dilatational (mode 1) fractures, and thrusts that overprint the originally formed structures (e.g. Alsop & Marco 2011). Explanations for this added structural heterogeneity have included the theory of multi-cell models, where a large, first-order MTC cell is composed of many transient secondary-order flow cells that locally interact and overprint related features (Alsop & Marco 2014). Similarly, identification of polyphase deformation/accumulation of multiple events from integrated seismic-field studies (e.g. Ogata et al. 2014) shows added intricacy when compared to the single-celled model assumption.

We suggest that, towards the eastern part of the MTC, compressional overprinting fabrics may have been preserved within a predominately extensional domain, as the fold-thrust system is seen much further updip. In addition, the longitudinal and sub-orthogonal shear zones represent velocity variations and potentially cell boundaries within a larger first-order MTC. Therefore, although extensional-translational-compressional sequences are often most appropriate when assessing MTC at a seismic scale, strain-overprinting should be considered together with strain analysis results. One potential way

to account for this complexity would be to treat each cell as a separate strain model. Identifying any strain discrepancies between and within cells could then be compared to the overall single-celled model.

7. CONCLUSIONS

(1) A structurally-complex Neogene MTC has been identified on the lower slope within the deep-water passive margin sequence, offshore Uruguay. Two potential emplacement models are proposed: (i) a shear coupling model, where an overriding debris flow(s) produced increased loading and localisation of shear stress on a mechanically weak zone, which subsequently underwent shear failure, or (ii) a loading process triggered the initial failure of sediment, with remnant topography being infilled by later unrelated debris flow(s).

(2) 3D seismic-reflection data, including several seismic attributes, enabled kinematic indictors to be determined from the following features: rafted-blocks, lateral margins and fold-thrust systems. In addition, two previously undocumented seismic kinematic indicators were identified: (1) sub-orthogonal shear zones, and (2) the formation of fold-thrust systems within the kinematic boundary zone beneath rafted-blocks. Characterisation of the MTC enabled a paleo-slope and transport direction to be identified and the correct orientation of strain analysis models to be constrained.

(3) This is the first study to undertake strain analysis, including quantification of intra-MTC strain, within a single, well-imaged MTC. The results reveal that, on a seismic-scale, the MTC does not balance, with 1.6-1.9 km (13-16% strain) extension and 6.8-7.5 km (17-18%) (c. 25% without the frontally emergent zone) contraction. A depth-dependant layer-parallel shortening is identified within the compressional domain that is consistent with other fold-thrust system models. One major uncertainty of the strain models is the missing components of sub-seismic/penetrative strain that are likely contributing significantly to shortening and extension.

(4) Using conventional seismic-analysis and classification the MTC could be split into a broadly tri-partite strain distribution with extensional, translational and compressional domains. However, after undertaking detailed seismic extractions and appreciating the limited nature of the translational domain, it is concluded that a bi-partite strain distribution, with an appreciation of strain overprinting processes, may be a more accurate way to describe many MTCs.

(5) The assumption of a structurally balanced MTC is a simple high-level concept. However, proving this based on natural examples is difficult due to a combination of the complex and often polyphase deformation history, and dataset limitations.

Acknowledgments

We thank two anonymous reviewers and the third reviewer Glenn Sharman for their constructive feedback which greatly improved the final submission, together with Cynthia Ebinger for editorial handling. Thank you to ANCAP and Shell for providing the dataset and allowing publication of the paper. Thank you to Schlumberger, ffA Geoteric and Midland Valley Exploration for software

donations. Thank you to Alexander Coleman for persisting in teaching Mike Steventon 2D Move and Marco Pizzi for his discussions on structural restoration techniques

REFERENCES

Alsop, G. & Holdsworth, R. 2007. Flow perturbation folding in shear zones. *Geological Society, London, Special Publications*, **272**, 75-101.

Alsop, G. & Marco, S. 2011. Soft-sediment deformation within seismogenic slumps of the Dead Sea Basin. *Journal of Structural Geology*, **33**, 433-457.

Alsop, G.I. & Marco, S. 2014. Fold and fabric relationships in temporally and spatially evolving slump systems: A multi-cell flow model. *Journal of Structural Geology*, **63**, 27-49.

Alsop, G.I., Weinberger, R. & Marco, S. 2018. Distinguishing thrust sequences in gravity-driven fold and thrust belts. *Journal of Structural Geology*.

Alves, T.M. 2015. Submarine slide blocks and associated soft-sediment deformation in deep-water basins: a review. *Marine and Petroleum Geology*, **67**, 262-285.

Alves, T.M. & Lourenço, S.D. 2010. Geomorphologic features related to gravitational collapse: Submarine landsliding to lateral spreading on a late Miocene–Quaternary slope (SE Crete, eastern Mediterranean). *Geomorphology*, **123**, 13-33.

Armandita, C., Morley, C.K. & Rowell, P. 2015. Origin, structural geometry, and development of a giant coherent slide: The South Makassar Strait mass transport complex. *Geosphere*, **11**, 376-403.

Armitage, D.A. & Stright, L. 2010. Modeling and interpreting the seismic-reflection expression of sandstone in an ancient mass-transport deposit dominated deep-water slope environment. *Marine and Petroleum Geology*, **27**, 1-12.

Bond, C., Gibbs, A., Shipton, Z. & Jones, S. 2007. What do you think this is?``Conceptual uncertainty''in geoscience interpretation. *GSA Today*, **17**, 4.

Bull, S., Cartwright, J. & Huuse, M. 2009. A review of kinematic indicators from mass-transport complexes using 3D seismic data. *Marine and Petroleum Geology*, **26**, 1132-1151.

Burberry, C.M. 2015. Spatial and temporal variation in penetrative strain during compression: Insights from analog models. *Lithosphere*, **7**, 611-624.

Butler, R. & Paton, D. 2010. Evaluating lateral compaction in deepwater fold and thrust belts: How much are we missing from “nature’s sandbox”. *GSA Today*, **20**, 4-10.

Butler, R.W., Eggenhuisen, J.T., Haughton, P. & McCaffrey, W.D. 2016. Interpreting syndepositional sediment remobilization and deformation beneath submarine gravity flows; a kinematic boundary layer approach. *Journal of the Geological Society of London*, **173**, 46-58.

Chopra, S. & Marfurt, K.J. 2008. Gleaning meaningful information from seismic attributes. *First Break*, **26**, 43-53.

Clare, M.A., Vardy, M.E., Cartigny, M.J., Talling, P.J., Himsworth, M.D., Dix, J.K., Harris, J.M., Whitehouse, R.J*., et al.* 2017. Direct monitoring of active geohazards: emerging geophysical tools for deep-water assessments. *Near Surface Geophysics*, **15**, 427-444.

Conti, B., de Jesus Perinotto, J.A., Veroslavsky, G., Castillo, M.G., de Santa Ana, H., Soto, M. & Morales, E. 2017. Speculative petroleum systems of the southern Pelotas Basin, offshore Uruguay. *Marine and Petroleum Geology*, **83**, 1-25.

Craddock, J.P. & van der Pluijm, B.A. 1989. Late Paleozoic deformation of the cratonic carbonate cover of eastern North America. *Geology*, **17**, 416-419.

Dahlstrom, C. 1969. Balanced cross sections. *Canadian Journal of Earth Sciences*, **6**, 743-757.

Dalton, T., Paton, D., Oldfield, S., Needham, D. & Wood, A. 2017. The importance of missing strain in Deep Water Fold and Thrust Belts. *Marine and Petroleum Geology*, **82**, 163-177.

Debacker, T.N., Dumon, M. & Matthys, A. 2009. Interpreting fold and fault geometries from within the lateral to oblique parts of slumps: a case study from the Anglo-Brabant Deformation Belt (Belgium). *Journal of Structural Geology*, **31**, 1525-1539.

Dott, R. 1963. Dynamics of subaqueous gravity depositional processes. *American Association of Petroleum Geologists (AAPG) Bulletin*, **47**, 104-128.

Farrell, S. 1984. A dislocation model applied to slump structures, Ainsa Basin, South Central Pyrenees. *Journal of Structural Geology*, **6**, 727-736.

Fleming, R.W. & Johnson, A.M. 1989. Structures associated with strike-slip faults that bound landslide elements. *Engineering Geology*, **27**, 39-114.

Fossen, H. 2016. *Structural geology*. Cambridge University Press.

Franke, D., Neben, S., Ladage, S., Schreckenberger, B. & Hinz, K. 2007. Margin segmentation and volcano-tectonic architecture along the volcanic margin off Argentina/Uruguay, South Atlantic. *Marine Geology*, **244**, 46-67.

Frey-Martínez, J., Cartwright, J. & James, D. 2006. Frontally confined versus frontally emergent submarine landslides: a 3D seismic characterisation. *Marine and Petroleum Geology*, **23**, 585-604.

Gamboa, D. & Alves, T.M. 2015. Three-dimensional fault meshes and multi-layer shear in mass-transport blocks: Implications for fluid flow on continental margins. *Tectonophysics*, **647**, 21-32.

Gamboa, D. & Alves, T.M. 2016. Bi-modal deformation styles in confined mass-transport deposits: Examples from a salt minibasin in SE Brazil. *Marine Geology*, **379**, 176-193.

Gauthier, B. & Lake, S. 1993. Probabilistic modeling of faults below the limit of seismic resolution in Pelican Field, North Sea, offshore United Kingdom. *AAPG Bulletin*, **77**, 761-777.

Gee, M., Gawthorpe, R. & Friedmann, J. 2005. Giant striations at the base of a submarine landslide. *Marine Geology*, **214**, 287-294.

Gee, M., Gawthorpe, R. & Friedmann, S. 2006. Triggering and evolution of a giant submarine landslide, offshore Angola, revealed by 3D seismic stratigraphy and geomorphology. *Journal of Sedimentary Research*, **76**, 9-19.

Groshong, R.H., Withjack, M.O., Schlische, R.W. & Hidayah, T.N. 2012. Bed length does not remain constant during deformation: Recognition and why it matters. *Journal of Structural Geology*, **41**, 86-97.

Heifetz, E., Agnon, A. & Marco, S. 2005. Soft sediment deformation by Kelvin Helmholtz Instability: A case from Dead Sea earthquakes. *Earth and Planetary Science Letters*, **236**, 497-504.

Henry, P., Jouniaux, L., Screaton, E.J., Hunze, S. & Saffer, D.M. 2003. Anisotropy of electrical conductivity record of initial strain at the toe of the Nankai accretionary wedge. *Journal of Geophysical Research: Solid Earth*, **108**.

Hodgson, D., Brooks, H., Ortiz-Karpf, A., Spychala, Y., Lee, D. & Jackson, C.-L. 2017. The entrainment and abrasion of megaclasts during submarine landsliding and their impact on flow behaviour. *Geological Society Special Publications*.

Hossack, J.R. 1979. The use of balanced cross-sections in the calculation of orogenic contraction: A review. *Journal of the Geological Society*, **136**, 705-711.

Hudec, M.R. & Jackson, M.P. 2004. Regional restoration across the Kwanza Basin, Angola: Salt tectonics triggered by repeated uplift of a metastable passive margin. *AAPG Bulletin*, **88**, 971-990.

Jackson, C.A. 2011. Three-dimensional seismic analysis of megaclast deformation within a mass transport deposit; implications for debris flow kinematics. *Geology*, **39**, 203-206.

Judge, P.A. & Allmendinger, R.W. 2011. Assessing uncertainties in balanced cross sections. *Journal of Structural Geology*, **33**, 458-467.

Kautz, S.A. & Sclater, J.G. 1988. Internal deformation in clay models of extension by block faulting. *Tectonics*, **7**, 823-832.

Knott, S.D., Beach, A., Brockbank, P.J., Brown, J.L., McCallum, J.E. & Welbon, A.I. 1996. Spatial and mechanical controls on normal fault populations. *Journal of Structural Geology*, **18**, 359-372.

Koyi, H. 1995. Mode of internal deformation in sand wedges. *Journal of Structural Geology*, **17**, 293297-295300.

Koyi, H.A., Sans, M., Teixell, A., Cotton, J. & Zeyen, H. 2004. The significance of penetrative strain in the restoration of shortened layers—Insights from sand models and the Spanish Pyrenees.

Krastel, S., Wefer, G., Hanebuth, T.J., Antobreh, A.A., Freudenthal, T., Preu, B., Schwenk, T., Strasser, M.*, et al.* 2011. Sediment dynamics and geohazards off Uruguay and the de la Plata River region (northern Argentina and Uruguay). *Geo-Marine Letters*, **31**, 271-283.

Lamarche, G., Joanne, C. & Collot, J.Y. 2008. Successive, large mass-transport deposits in the south Kermadec fore-arc basin, New Zealand: The Matakaoa Submarine Instability Complex. *Geochemistry, Geophysics, Geosystems*, **9**.

Lewis, K. 1971. Slumping on a continental slope inclined at 1–4. *Sedimentology*, **16**, 97-110.

Lingrey, S. & Vidal-Royo, O. 2015. Evaluating the quality of bed length and area balance in 2D structural restorations. *Interpretation*, **3**, SAA133-SAA160.

Marrett, R. & Allmendinger, R.W. 1992. Amount of extension on" small" faults: An example from the Viking graben. *Geology*, **20**, 47-50.

Martinsen, O. 1994. Mass movements *The geological deformation of sediments*. Springer, 127-165.

Martinsen, O.J. & Bakken, B. 1990. Extensional and compressional zones in slumps and slides in the Namurian of County Clare, Ireland. *Journal of the Geological Society*, **147**, 153-164.

Masson, D., Huggett, Q. & Brunsden, D. 1993. The surface texture of the Saharan debris flow deposit and some speculations on submarine debris flow processes. *Sedimentology*, **40**, 583-598.

Meckel, L. 2011. Reservoir characteristics and classification of sand-prone submarine mass-transport deposits. *SEPM Special Publication*, **96**, 432-452.

Merle, O. 1989. Strain models within spreading nappes. *Tectonophysics*, **165**, 57-71.

Moore, Z.T. & Sawyer, D.E. 2016. Assessing post-failure mobility of submarine landslides from seismic geomorphology and physical properties of mass transport deposits: An example from seaward of the Kumano Basin, Nankai Trough, offshore Japan. *Marine Geology*, **374**, 73-84.

Morales, E., Chang, H.K., Soto, M., Corrêa, F.S., Veroslavsky, G., de Santa Ana, H., Conti, B. & Daners, G. 2017. Tectonic and stratigraphic evolution of the Punta del Este and Pelotas basins (offshore Uruguay). *Petroleum Geoscience*, petgeo2016-2059.

Morita, S., Nakajima, T. & Hanamura, Y. 2011. Submarine slump sediments and related dewatering structures: observations of 3D seismic data obtained for the continental slope off Shimokita Peninsula, NE Japan. *NE Japan. Journal of the Geological Society of Japan*, **117**, 95-98.

Moscardelli, L. & Wood, L. 2015. Morphometry of mass-transport deposits as a predictive tool. *Geological Society of America Bulletin*, B31221. 31221.

Moscardelli, L., Wood, L. & Mann, P. 2006. Mass-transport complexes and associated processes in the offshore area of Trinidad and Venezuela. *AAPG Bulletin*, **90**, 1059-1088.

Nardin, T.R. 1979. A review of mass movement processes sediment and acoustic characteristics, and contrasts in slope and base-of-slope systems versus canyon-fan-basin floor systems. *SEPM Special Publication*.

Nemec, W. 1990. Aspects of sediment movement on steep delta slopes. *Special Publication, International Association of Sedimentologists, Coarse-grained deltas*, **10**, 29-73.

Nürnberg, D. & Müller, R.D. 1991. The tectonic evolution of the South Atlantic from Late Jurassic to present. *Tectonophysics*, **191**, 27-53.

Ogata, K., Mountjoy, J., Pini, G.A., Festa, A. & Tinterri, R. 2014. Shear zone liquefaction in mass transport deposit emplacement: A multi-scale integration of seismic reflection and outcrop data. *Marine Geology*, **356**, 50-64.

Ortiz-Karpf, A., Hodgson, D.M., Jackson, C.A.L. & McCaffrey, W.D. 2018. Mass-transport complexes as markers of deep-water fold-and-thrust belt evolution: insights from the southern M agdalena fan, offshore C olombia. *Basin Research*, **30**, 65-88.

Partyka, G., Gridley, J. & Lopez, J. 1999. Interpretational applications of spectral decomposition in reservoir characterization. *The Leading Edge*, **18**, 353-360.

Pickering, K.T. & Corregidor, J. 2005. Mass-transport complexes (MTCs) and tectonic control on basin-floor submarine fans, middle Eocene, south Spanish Pyrenees. *Journal of Sedimentary Research*, **75**, 761-783.

Posamentier, H.W. & Kolla, V. 2003. Seismic geomorphology and stratigraphy of depositional elements in deep-water settings. *Journal of Sedimentary Research*, **73**, 367-388.

Posamentier, H.W. & Martinsen, O.J. 2011. The character and genesis of submarine mass-transport deposits: insights from outcrop and 3D seismic data. *Mass-transport deposits in deepwater settings: Society for Sedimentary Geology (SEPM) Special Publication 96*, 7-38.

Prior, D.B., Bornhold, B.D. & Johns, M. 1984. Depositional characteristics of a submarine debris flow. *The Journal of Geology*, **92**, 707-727.

Rabinowitz, P.D. & LaBrecque, J. 1979. The Mesozoic South Atlantic Ocean and evolution of its continental margins. *Journal of Geophysical Research: Solid Earth*, **84**, 5973-6002.

Randen, T. 1998. Automated Stratigraphic and Fault Interpretation. PCT Patent Application No PCT/IB99/01040.

Randen, T. & Sønneland, L. 2005. Atlas of 3D Seismic Attributes. *In*: Iske, A. & Randen, T. (eds) *Mathematical Methods and Modelling in Hydrocarbon Exploration and Production*. Springer Berlin Heidelberg, Berlin, Heidelberg, 23-46.

Randen, T., Pedersen, S.I. & Sønneland, L. 2001. Automatic extraction of fault surfaces from three-dimensional seismic data *SEG Technical Program Expanded Abstracts 2001*. Society of Exploration Geophysicists, 551-554.

Rowan, M.G., Peel, F.J. & Vendeville, B.C. 2004. Gravity-driven fold belts on passive margins.

Schlische, R.W., Groshong, R.H., Withjack, M.O. & Hidayah, T.N. 2014. Quantifying the geometry, displacements, and subresolution deformation in thrust-ramp anticlines with growth and erosion: From models to seismic-reflection profile. *Journal of Structural Geology*, **69**, 304-319.

Schnellmann, M., Anselmetti, F.S., Giardini, D. & McKENZIE, J.A. 2005. Mass movement-induced fold-and-thrust belt structures in unconsolidated sediments in Lake Lucerne (Switzerland). *Sedimentology*, **52**, 271-289.

Sclater, J.G. & Christie, P.A. 1980. Continental stretching: An explanation of the post-Mid-Cretaceous subsidence of the central North Sea Basin. *Journal of Geophysical Research: Solid Earth*, **85**, 3711-3739.

Sharman, G.R., Graham, S.A., Masalimova, L.U., Shumaker, L.E. & King, P.R. 2015. Spatial patterns of deformation and paleoslope estimation within the marginal and central portions of a basin-floor mass-transport deposit, Taranaki Basin, New Zealand. *Geosphere*, **11**, 266-306.

Sharman, G.R., Schwartz, T.M., Shumaker, L.E., Trigg, C.R., Nieminski, N.M., Sickmann, Z.T., Malkowski, M.A., Hourigan, J.K.*, et al.* 2017. Submarine mass failure within the deltaic Domengine Formation (Eocene), California (USA). *Geosphere*, **13**, 950-973.

Sobiesiak, M.S., Alsop, G.I., Kneller, B. & Milana, J.P. 2017. Sub-seismic scale folding and thrusting within an exposed mass transport deposit: A case study from NW Argentina. *Journal of Structural Geology*, **96**, 176-191.

Soto, M., Morales, E., Veroslavsky, G., de Santa Ana, H., Ucha, N. & Rodríguez, P. 2011. The continental margin of Uruguay: Crustal architecture and segmentation. *Marine and Petroleum Geology*, **28**, 1676-1689.

Strachan, L. & Alsop, G.I. 2006. Slump folds as estimators of palaeoslope: a case study from the Fisherstreet Slump of County Clare, Ireland. *Basin Research*, **18**, 451-470.

Van Bemmel, P.P. & Pepper, R.E. 2000. Seismic signal processing method and apparatus for generating a cube of variance values. Google Patents.

Van der Merwe, W., Hodgson, D. & Flint, S. 2009. Widespread syn-sedimentary deformation on a muddy deep-water basin-floor: the Vischkuil Formation (Permian), Karoo Basin, South Africa. *Basin Research*, **21**, 389-406.

Van Der Merwe, W.C., Hodgson, D.M. & Flint, S.S. 2011. Origin and terminal architecture of a submarine slide: a case study from the Permian Vischkuil Formation, Karoo Basin, South Africa. *Sedimentology*, **58**, 2012-2038.

Varnes, D.J. 1978. Slope movement types and processes. *Special report*, **176**, 11-33.

Walsh, J., Watterson, J., Childs, C. & Nicol, A. 1996. Ductile strain effects in the analysis of seismic interpretations of normal fault systems. *Geological Society, London, Special Publications*, **99**, 27-40.

Wang, F., Dai, Z. & Zhang, S. 2017. Experimental study on the motion behavior and mechanism of submarine landslides. *Bulletin of Engineering Geology and the Environment*, 1-10.

Watt, S., Talling, P., Vardy, M., Masson, D., Henstock, T., Hühnerbach, V., Minshull, T., Urlaub, M.*, et al.* 2012. Widespread and progressive seafloor-sediment failure following volcanic debris avalanche emplacement: Landslide dynamics and timing offshore Montserrat, Lesser Antilles. *Marine Geology*, **323**, 69-94.

Weimer, P. 1990. Sequence Stratigraphy, Facies Geometries, and Depositional History of the Mississippi Fan, Gulf of Mexico (1). *American Association of Petroleum Geologists (AAPG) bulletin*, **74**, 425-453.

Weimer, P. & Shipp, C. 2004. Mass transport complex: musing on past uses and suggestions for future directions. *Offshore Technology Conference*. Offshore Technology Conference.

Wetzler, N., Marco, S. & Heifetz, E. 2010. Quantitative analysis of seismogenic shear-induced turbulence in lake sediments. *Geology*, **38**, 303-306.

Zeng, H., Henry, S.C. & Riola, J.P. 1998. Stratal slicing, part II: Real 3-D seismic data. *Geophysics*, **63**, 514-522.

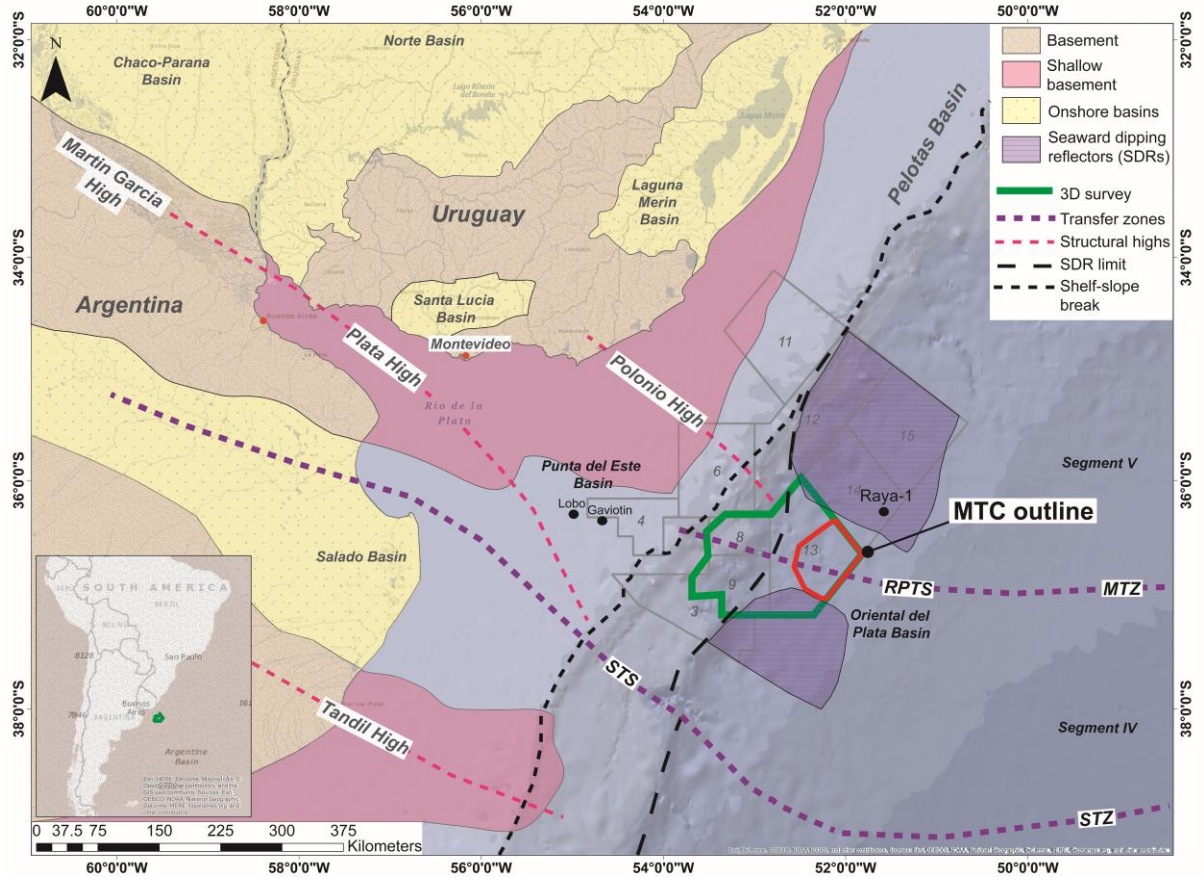

Figure 1: Study area offshore Uruguay, onshore/offshore basins outlines and structural highs from ANCAP and (Soto et al. 2011), landward limit of seaward dipping reflectors from (Franke et al. 2007), note current licence blocks and Lobo and Gaviotin wells, dataset (green) and study area (red) outlines, Raya-1 location from spectrumgeo.

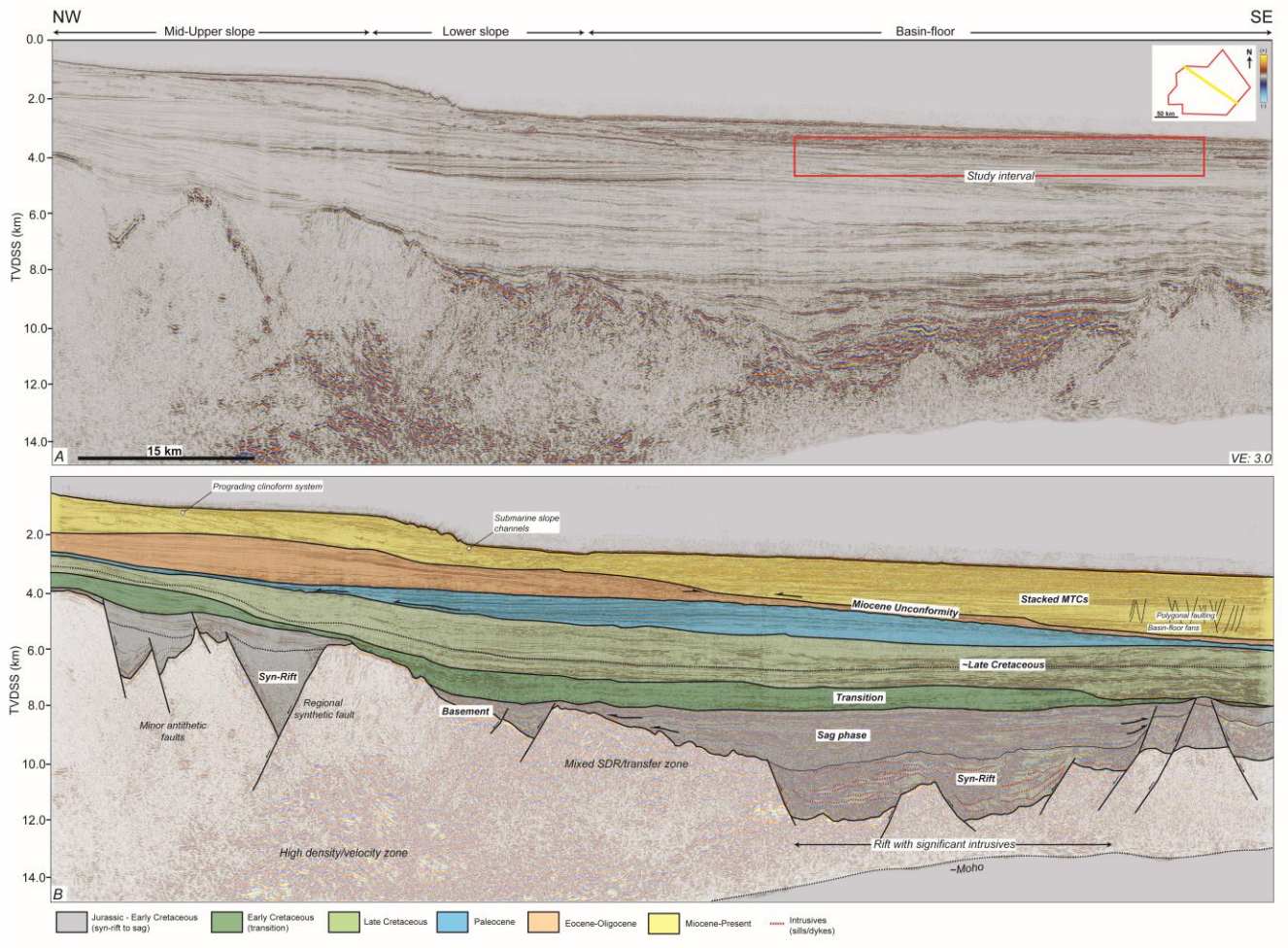

Figure 2: (A) Dip seismic section, (B) geosection, through the central Uruguay margin spanning the continental to transitional crust with significant volcanic components including SDRs, a high density underplating zone and intrusives. Stratigraphic ages are estimated from (Morales et al. 2017) and ANCAP. Note the study area, located down-dip from a large prograding clinoform system.

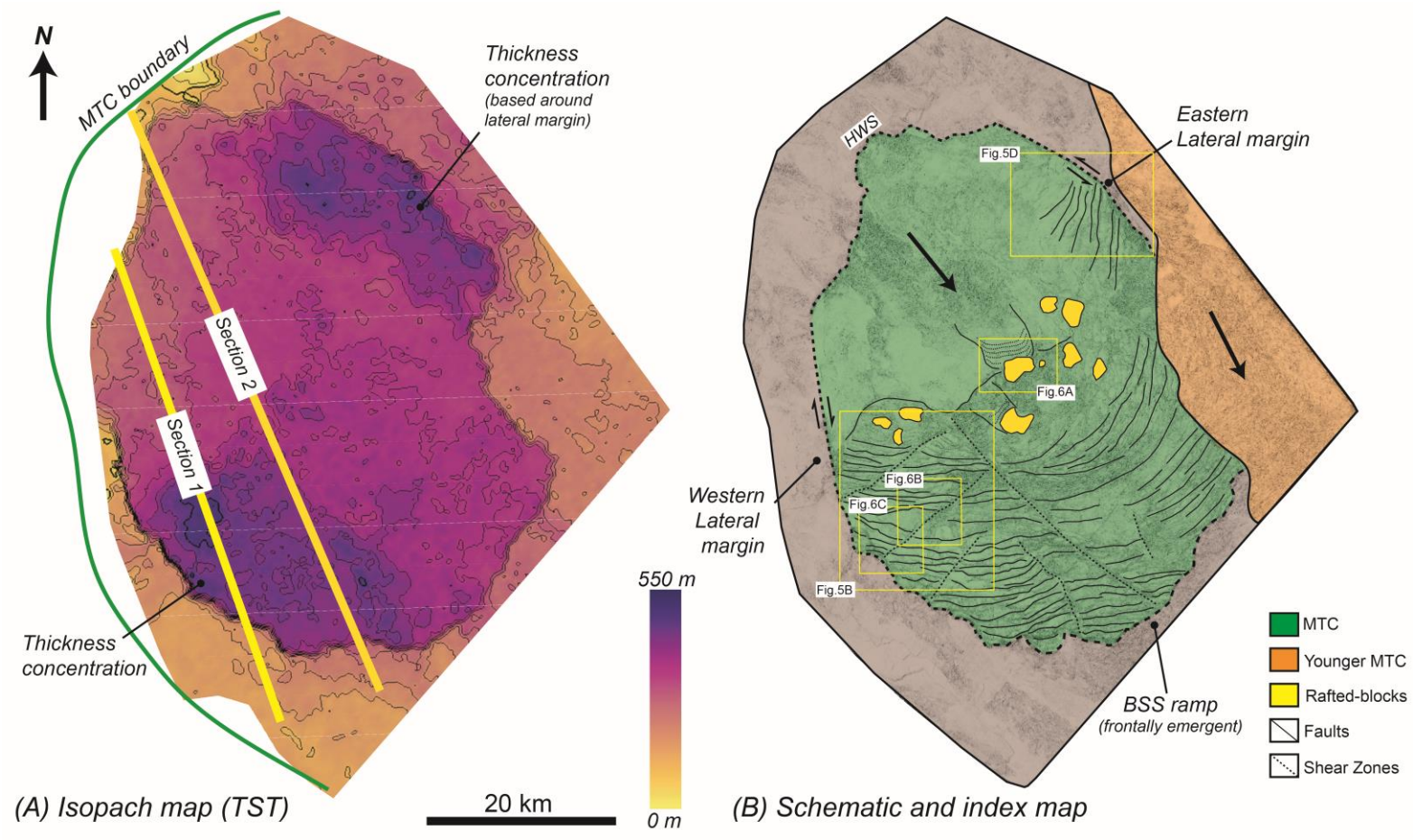

Figure 3: (A) Isopach map displayed in true stratigraphic thickness, between the basal shear surface (BSS) and top surface. Note Sections 1 and 2 which are the dip sections chosen for strain analysis, (B) Schematic and index map of main structural elements within the MTC and reference locations for later figures.

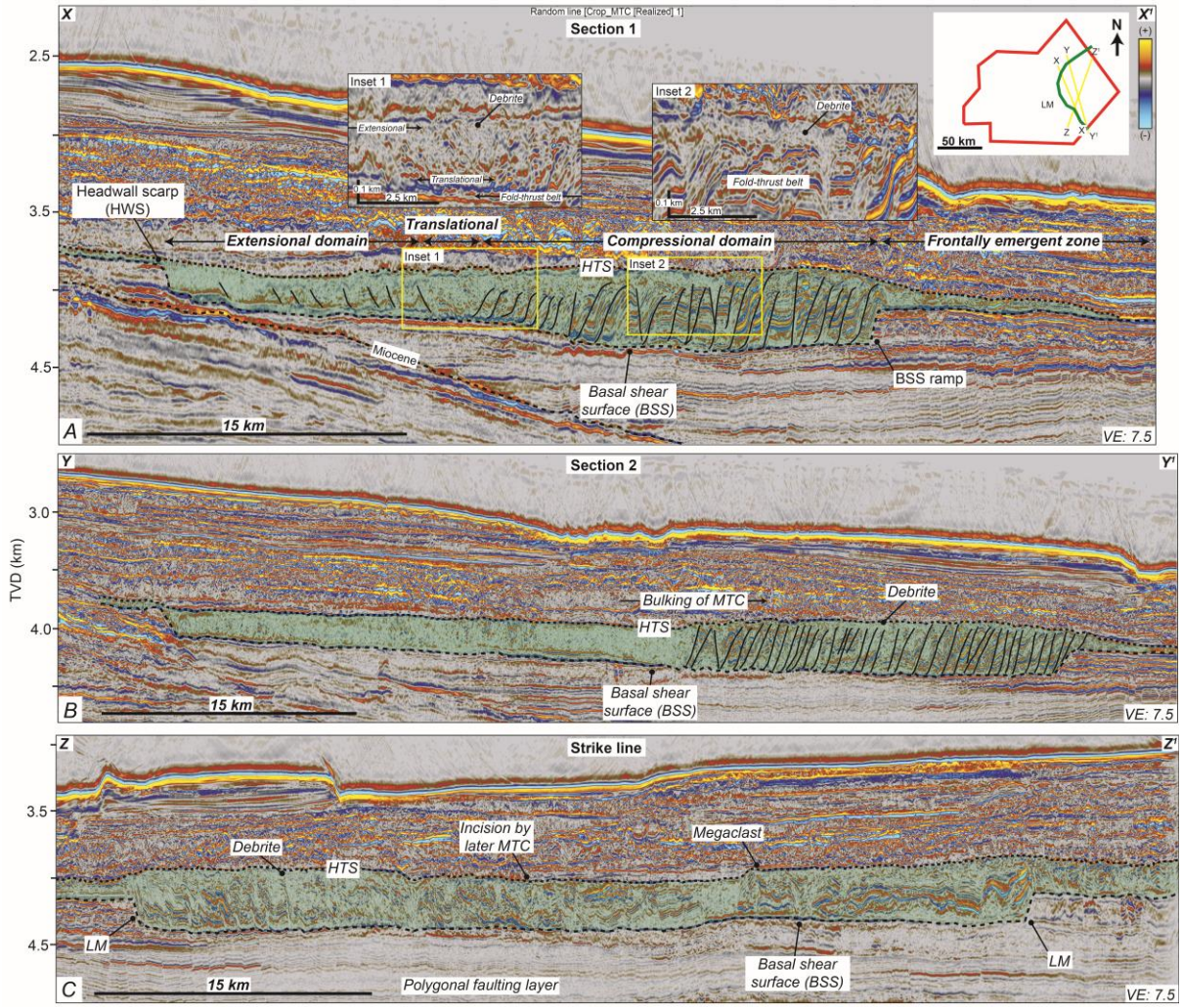

Figure 4. (A) Dip seismic Section 1, used for structural restoration, note the well-defined extensional and compressional domains, and inset sections highlighting the overriding debrite, (B) Dip seismic Section 2 used for structural restoration located more centrally within the MTC note bulking towards the compressional domain, (C) Strike seismic section highlighting distinct lateral margins, megaclasts and incision of the top surface, HTS = hummocked top surface, LM = lateral margins. Amplitudes have been compressed to account for washout from very high amplitude gas charged sediment above the study interval.

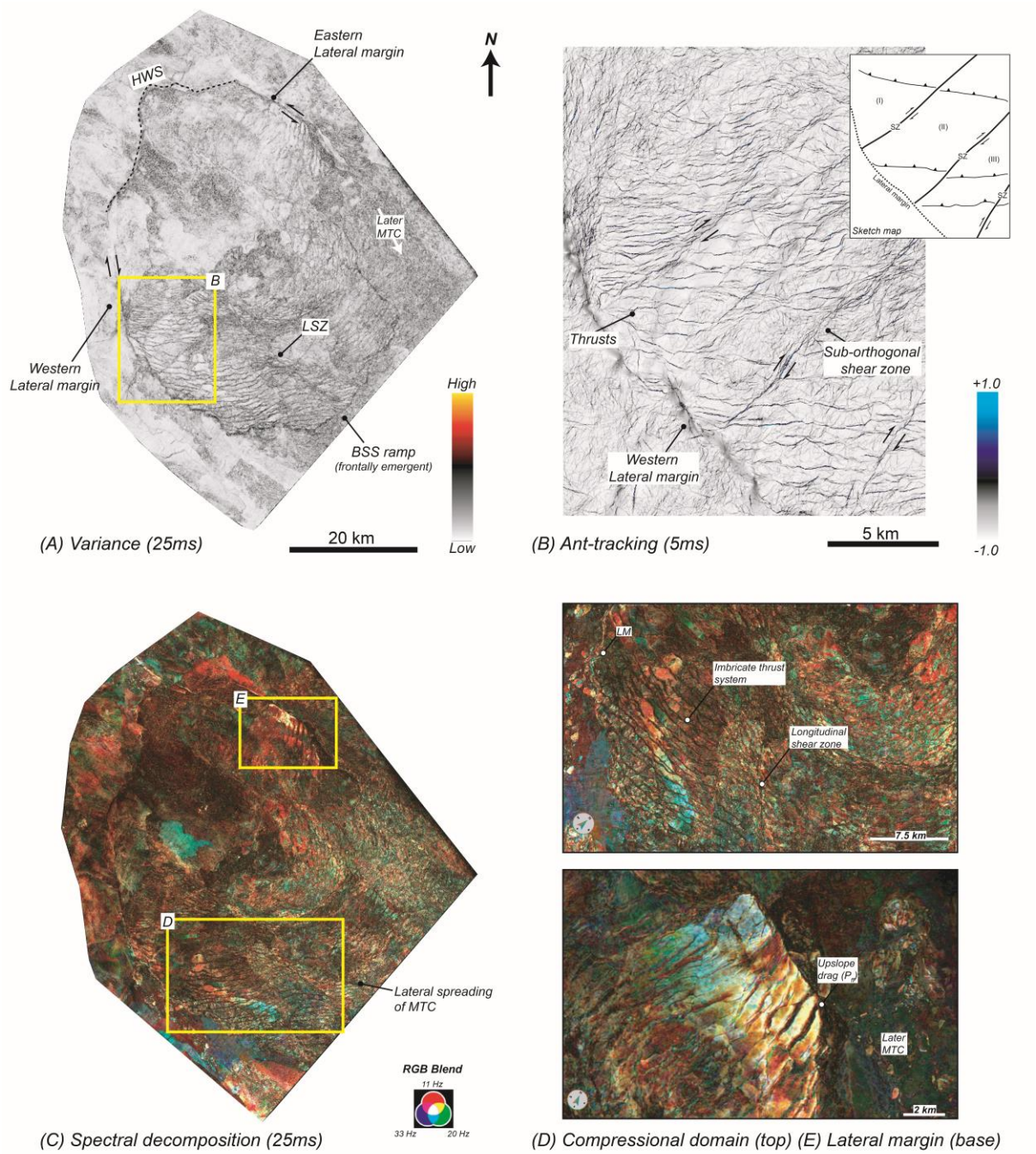

Figure 5: (A) Variance extraction from the basal shear surface over a 25ms window, delineating the lateral margins, frontally emergent ramp and longitudinal shear zone (LSZ), (B) Ant-track extraction from the basal shear surface over 5ms, imaging the interaction between the western lateral margin and sub-orthogonal shear zones, (C) Spectral decomposition extraction from the basal shear surface over a 25ms window, note locations of D and E, (D) Compressional domain imaging imbricate thrust systems, (E) Eastern lateral margin imaging upslope drag and erosion by a younger MTC.

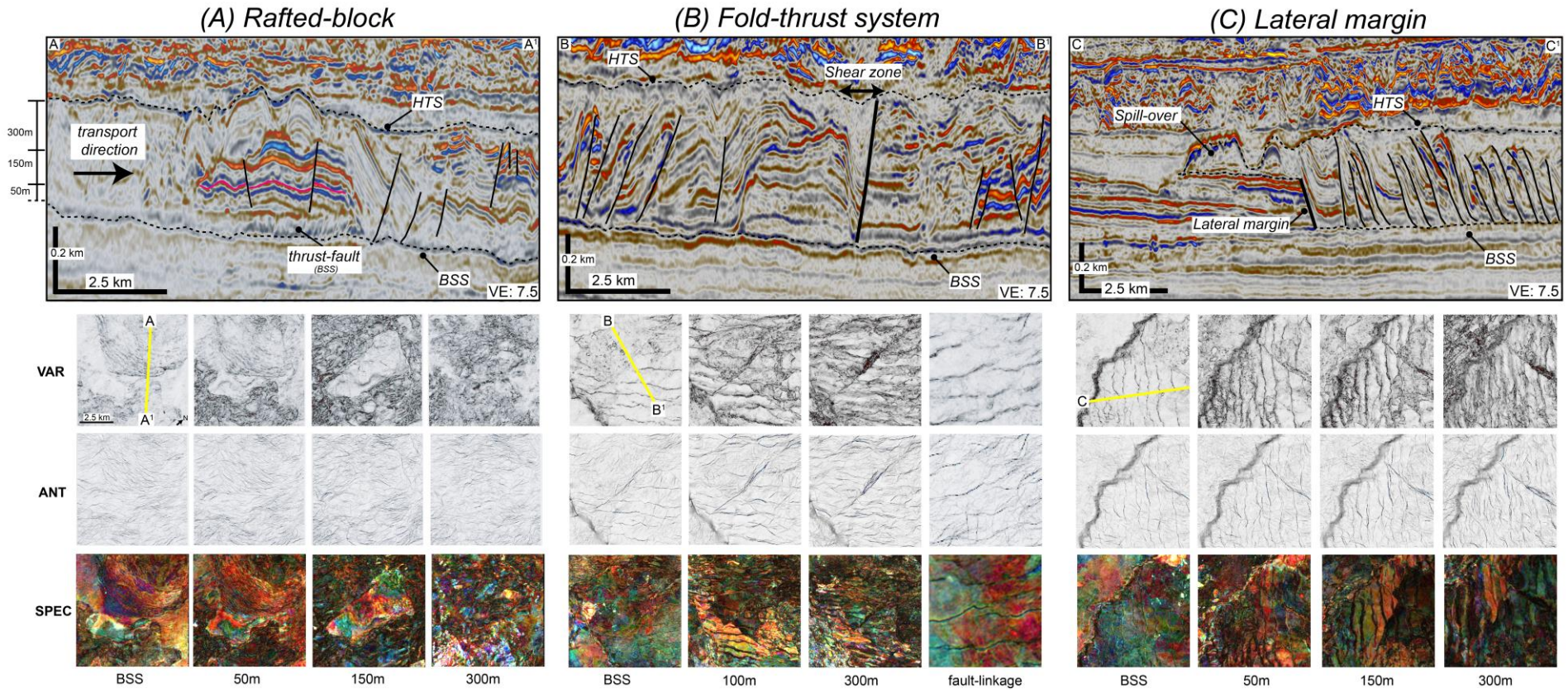

Figure 6: Iso-proportional variance (VAR), ant-track (ANT) and spectral decomposition (SPEC) extractions between the BSS and top surface (HTS), (A) Seismic dip line displaying rafted-block, BSS thrust faults and intra-block normal faults, BSS to 300m above demonstrating the through going nature of the fault systems, (B) Seismic line through MTC thrust-fault system and orthogonal shear zone seen to detach onto the BSS, fault linkage (relay ramps) imaged between thrust faults, (C) Seismic line highlighting the abrupt western lateral margin, note the irregular nature of the thrust as they interact with the lateral margin.

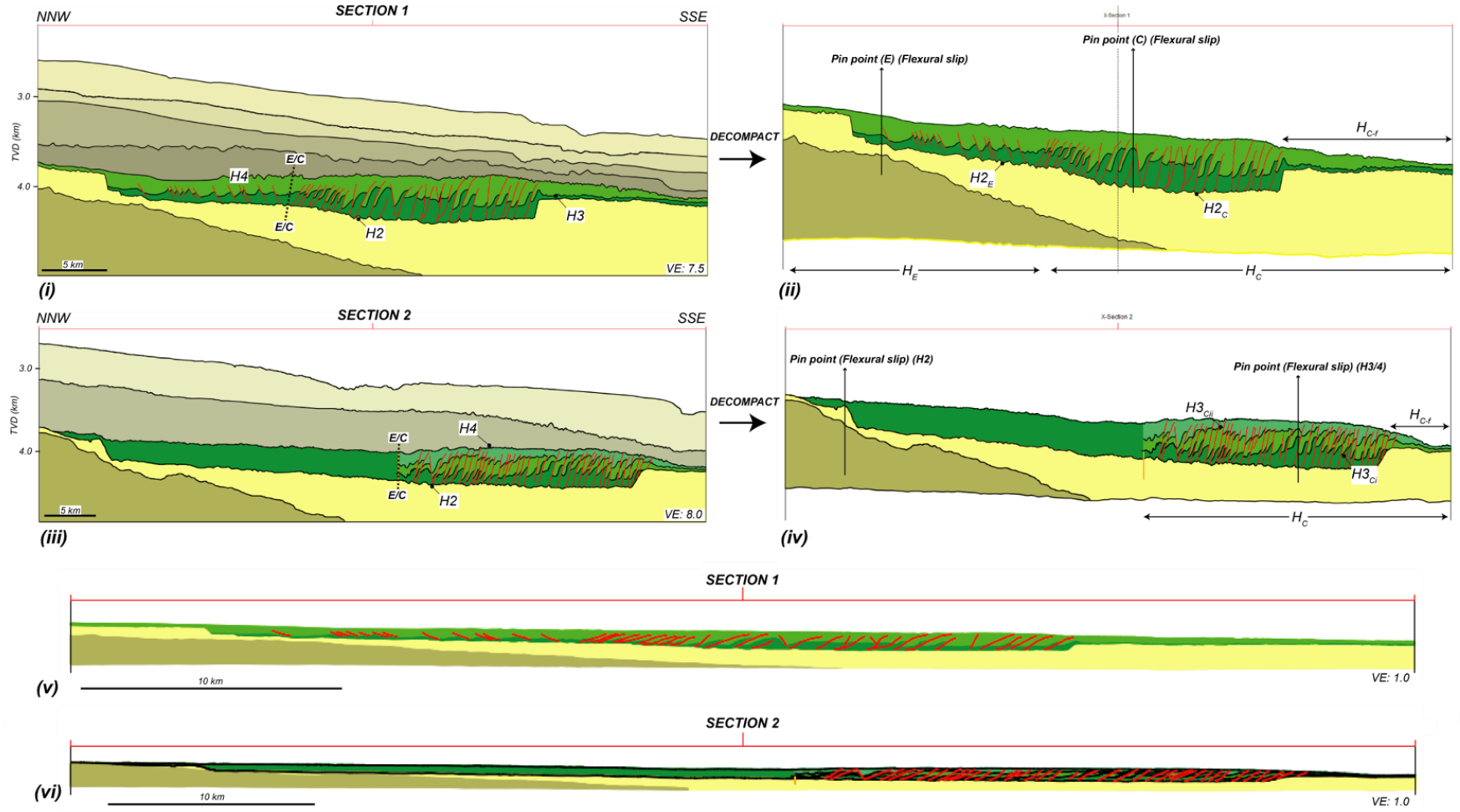

Figure 7: Decompacted strain analysis models, (i) Section 1 present day section, (ii) Section 1 decompacted section, (iii) Section 2 present day section, (iv) Section 2 decompacted section. Section 1 sits near the western lateral margin of the MTC, Section 2 crosses centrally through the main MTC body, note pin points used for flexural slip calculations, (v/vi) Vertically exaggeration 1.0.

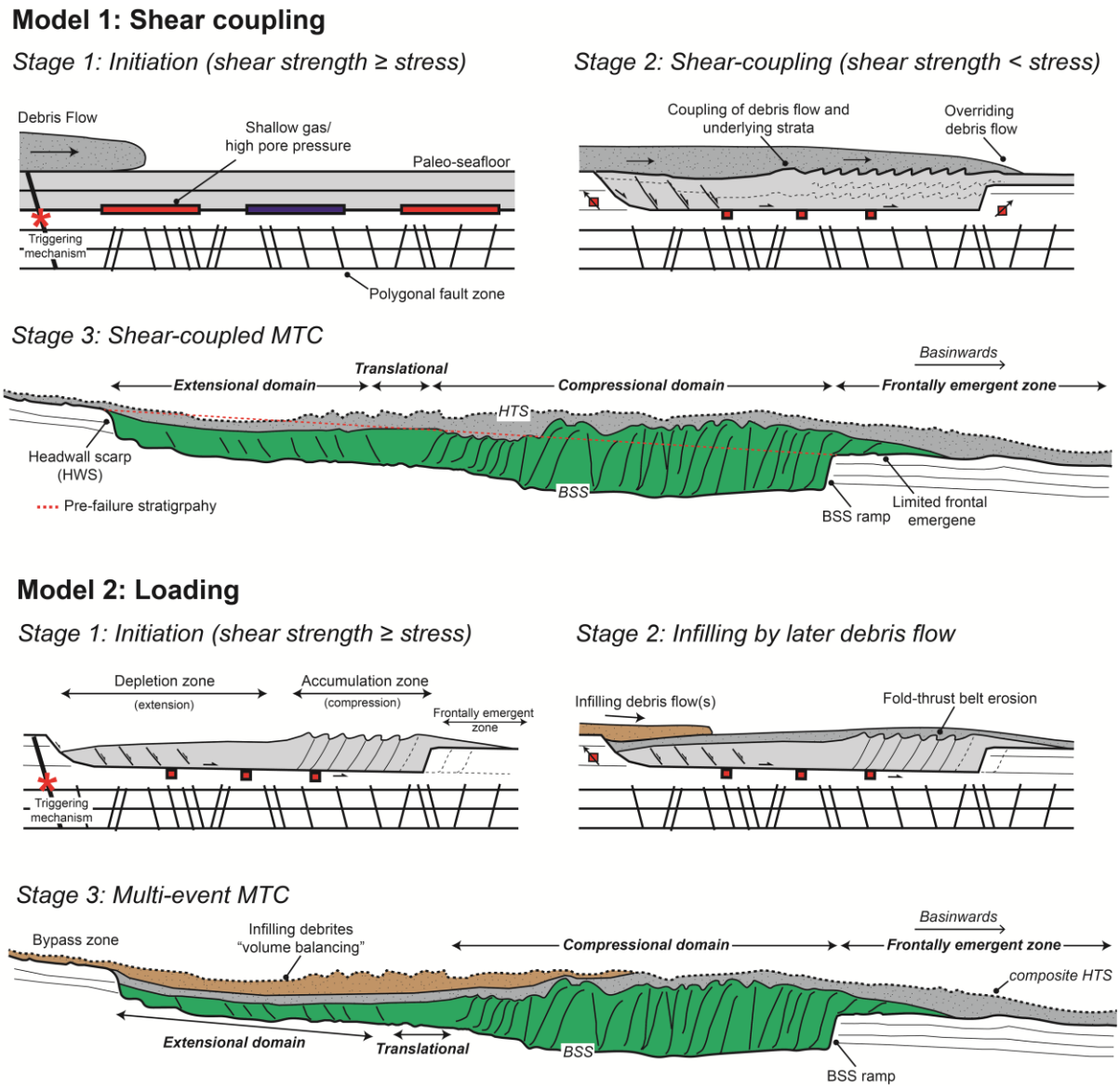

Figure 8: MTC emplacement models, Model 1: Shear coupling mechanism, stage 1 initiation through overriding debris flow producing localisation of shear stress on a mechanically weak likely shallow gas filled zone, stage 2 in situ failure of underlying sediments through shear coupling, stage 3 failure of underlying sediments has produced significant extensional and compressional domains in the final deposit, Model 2: Loading mechanism, stage 1 initiation through loading and progressive downslope failure, stage 2 infilling of remnant topography by later debris flow(s), stage 3 failure from a loading mechanism has produced similar extensional and compressional domains to Model 1.

55 *Table 1: Results of strain analysis, positive values indicate extension, negative values indicate compression.*

Restoration Method	***Horizon***	***Present-length (m)***	***Restored-length (m)***	***Missing length (m)***	***Strain (e)***
Section 1					
Line-length	H2	51600	52024	424	*-0.8*
	H3	46206	51827	5621	*-10.8*
	H4	51600	51708	108	*-0.2*
	$H3_E$	13900	12002	-1898	*15.8*
	$H3_C$	32345	39824	7480	*-18.8*
	$H3_{C-f}$	20585	27983	7398	*-26.4*
Simple/vertical shear (90 deg)	H2	51600	51602	2	*0.0*
	H3	46206	51058	4852	*-9.5*
	H4	51600	51598	-2	*0.0*
	$H3_E$	13900	12218	-1682	*13.8*
	$H3_C$	32345	39152	6808	*-17.4*
	$H3_{C-f}$	20585	27359	6774	*-24.8*
Flexural slip	H2	51600	52024	424	*-0.8*
	H3	46206	51826	5620	*-10.8*
	H4	51600	51708	108	*-0.2*
	$H3_E$	13900	12316	-1584	*12.9*
	$H3_C$	32345	39825	7481	*-18.8*
	$H3_{C-f}$	20585	27982	7397	*-26.4*
Section 2					
Line-length	H2	65000	65675	675	*-1.0*
	H4	63800	64404	604	*-0.9*
	$H3_{Ci}$	24058	32894	8836	-26.9
	$H3_{Cii}$	30028	35404	5376	-15.2
	$H3_{Cii-f}$	23963	29056	5093	-17.5
Simple shear (unfold 90 deg)	H2	65000	65028	28	0.0
	H4	63800	63836	36	-0.1
	$H3_{Ci}$	24058	31812	7754	-24.4
	$H3_{Cii}$	30028	34922	4894	-14.0
	$H3_{Cii-f}$	23963	28593	4630	-16.2
Flexural slip	H2	65000	65681	681	-1.0
	H4	63800	64460	660	-1.0
	$H3_{Ci}$	24058	32895	8837	-26.9
	$H3_{Cii}$	30028	35404	5376	-15.2
	$H3_{Cii-f}$	23963	29057	5094	-17.5

56

57

58

Table 2: Recalculating of strain assuming isoclinal folding in the compressional domain. Note the significant increase in shortening when compared to Table.1.

Restoration Method	***Horizon***	***Present-length (m)***	***Restored-length (m)***	***Missing length (m)***	***Strain (e)***
Section 1 - Isoclinal assumption					
Line Length	$H3_C$	32345	57642	25298	*-43.9*
	$H3_{C-f}$	20585	44920	24335	*-54.2*